Supplementary Materials

Text S1. Models for Fitting Removal Kinetics

The four kinetic models used in the present study, including the pseudo-first order, pseudo-second order, intraparticle diffusion and Elovich models, can be described as follows:

$$\log(q_e - q_t) = \log q_e - \frac{k_1 t}{2.303} \quad (1)$$

$$\frac{t}{q_t} = \frac{1}{k_e q_e^2} + \frac{t}{q_e} \quad (2)$$

$$q_t = k_3 t^{0.5} + B \quad (3)$$

$$q_t = \frac{1}{\beta}\ln(\alpha\beta) + \frac{1}{\beta}\ln t \quad (4)$$

where q_e and q_t represent the quantity of dye removal at equilibrium and at time t, respectively; k_1 (1/min), k_2 (g/mg/min) and k_3 (mg/g $min^{0.5}$) stand for the rate constants of pseudo-first-order kinetic model, pseudo-second-order kinetic model and intraparticle diffusion model, respectively; B is the intercept that is associated to the boundary layer thickness, α (mg/g/min) represents an initial removal rate and β (g/mg) is a desorption constant.

The pseudo-first-order kinetic model describes the rate of removal to be proportional to the number of unoccupied active sites by the solutes, while the pseudo-second-order kinetic model assumes that the removal rate of dye is proportional with the square of difference between the quantity of dye removed with time and the amount of dye absorbed at equilibrium [1]. The intraparticle diffusion model hypothesizes that the solute uptake changes proportionally with $t^{0.5}$ rather than with the contact time t [2]. The Elovich model was generally applied in chemisorption kinetics, which was found in overlapping a broad range of slow adsorption rate [3].

Text S2. Isotherms Study

The equilibrium adsorption data were fitted using four commonly used isotherm models, including Langmuir, Freundlich, Temkin, and Dubinin-Radushkevich (D-R) isotherms.

The Langmuir isotherm assumes that the adsorption sites are monolayer and identically homogeneous adsorption on the outer surface of adsorbent with a finite number of adsorption sites, which can be expressed as follows:

$$\frac{C_e}{q_e} = \frac{1}{k_L q_{max}} + \frac{C_e}{q_{max}} \quad (5)$$

where k_L represents the Langmuir adsorption equilibrium constant (L/g), q_{max} stands for the maximum adsorption (mg/g). In addition, the essential feature of the Langmuir isotherm can be evaluated by means of R_L, which is given as follows:

$$R_L = \frac{1}{1 + k_L C_0} \quad (6)$$

The Freundlich model is applied to describe the adsorption process onto the heterogeneous adsorption sites with different affinities on the surface of adsorbent and with the distinct interactions with sobates [4].

$$\log q_e = \log K_F + \frac{1}{n}\log C_e \quad (7)$$

where K_F and n stand for the Freundlich constants related to adsorption intensity and adsorption capacity, respectively. The 1/n value between 0 and 1 indicated that the adsorption processes of the sorbate were favorable.

The Temkin isotherm supposes that the heat of adsorption process decreases linearly as the degree of adsorption increases [5], which can be represented by the following equation:

$$q_e = \frac{RT}{a_t}\ln b_t + \frac{RT}{a_t}\ln C_e \quad (8)$$

where RT/a_t and b_t are the constants related to the heat (J/mol) and binding energy (L/g) of the adsorption process.

The experimental data were also fitted to the D-R isotherm to evaluate the nature of the adsorption process as physical or chemical, which can be expressed as follows:

$$\ln q_e = \ln q_{max} - \alpha\varepsilon^2 \quad (9)$$

$$\varepsilon = RT\ln(1+\frac{1}{C_e}) \quad (10)$$

$$E = 2\alpha^{-1/2} \quad (11)$$

where α represents the activity coefficient related to adsorption mean free energy (mol^2/J^2), ε stands for the Polanyi potential and E (kJ/mol) is the mean energy of adsorption.

Table S1. Parameters of porous structure of nanocomposites.

	nZVI	GO	rGOA	rGOA-nZVI-1	rGOA-nZVI-2	rGOA-nZVI-3	rGOA-nZVI-4	rGOA-nZVI-5
Surface area (m^2/g)	5.49	94.9	83.2	20.9	16.9	35.5	31.6	22.7
Pore diameter (nm)	3.83	3.83	2.19	3.82	3.82	3.84	3.83	3.83

Table S2. Adsorption kinetic parameters for MB and MO removal by rGOA-nZVI nanocomposites.

Model	Parameters	MB	MO
Pseudo-first-order kinetic	$k_1(min^{-1})$	0.156	0.151
	q_e(calc) ($mg•g^{-1}$)	509	575
	R^2	0.915	0.884
Pseudo-second-order kinetic	k_2 (g•mg-1•min^{-1})	0.00200	0.00120
	q_e (calc) ($mg•g^{-1}$)	826	341
	R^2	0.999	0.999
Intraparticle diffusion	K_{1d} ($mg•g^{-1}•min^{-1/2}$)	134	55.0
	C_1 ($mg•g^{-1}$)	380	103
	R^2	0.959	0.982
Elovich	K_{2d}($mg•g^{-1}•min^{-1/2}$)	3.09	4.60
	C_2 ($mg•g^{-1}$)	794	294
	R^2	0.804	0.804
	B ($g•mg^{-1}$)	0.0149	0.0240
	α($mg•g^{-1}•min^{-1}$)	$3.07*10^6$	2322
	R^2	0.817	0.951
	q_e (exp) ($mg•g^{-1}$)	819	332

Table S3. Sorption isotherm parameters for the removal of MB and MO by rGOA-nZVI nanocomposites.

Isotherms	Parameters	MB	MO	x^2	APE	SAE
Langmuir	K_L (L/mg)	0.0700	0.170	50.8 (MB) 3.42 (MO)	0.0400 (MB) 0.0300 (MO)	631 (MB) 97.3 (MO)
	q_{max} (mg/g)	3918	667			
	R^2	0.999	0.992			
Freundlich	K_F (mg/g)	916	314	913 (MB) 7.26 (MO)	0.200 (MB) 0.04 (MO)	3993 (MB) 153 (MO)
	n	4.22	6.42			
	$1/n$	0.240	0.160			
	R^2	0.802	0.961			
Temkin	RT/a_t(kJ/mol)	522	73.8	358 (MB) 15.7 (MO)	0.140 (MB) 0.0700 (MO)	2328 (MB) 216 (MO)
	b_t (L/g)	3.06	53.6			
	R^2	0.910	0.920			
D-R	q_m (mg/g)	3228	3459	782 (MB) 91.5 (MO)	0.170 (MB) 0.130 (MO)	3533 (MB) 428 (MO)
	α (mol^2/J^2)	4E^{-6}	8E^{-6}			
	E (kJ/mol)	1.00	0.71			
	R^2	0.843	0.881			
Experimental q_{max}(mg/g)				3877 (MB) 631 (MO)		

Table S4. The thermodynamic parameters of MB and MO removal by rGOA-nZVI nanocomposites.

	ΔS^0(kJ/mol/K)	ΔH^0(kJ/mol)	ΔG^0(kJ/mol)				
MB	0.130	30.5	288 K	298 K	308 K	318 K	328 K
			-5.09	-9.19	-11.9	-10.5	-10.5
MO	0.210	53.1	288 K	298 K	308 K	318 K	328 K
			-7.74	-9.84	-11.1	-12.5	-15.2

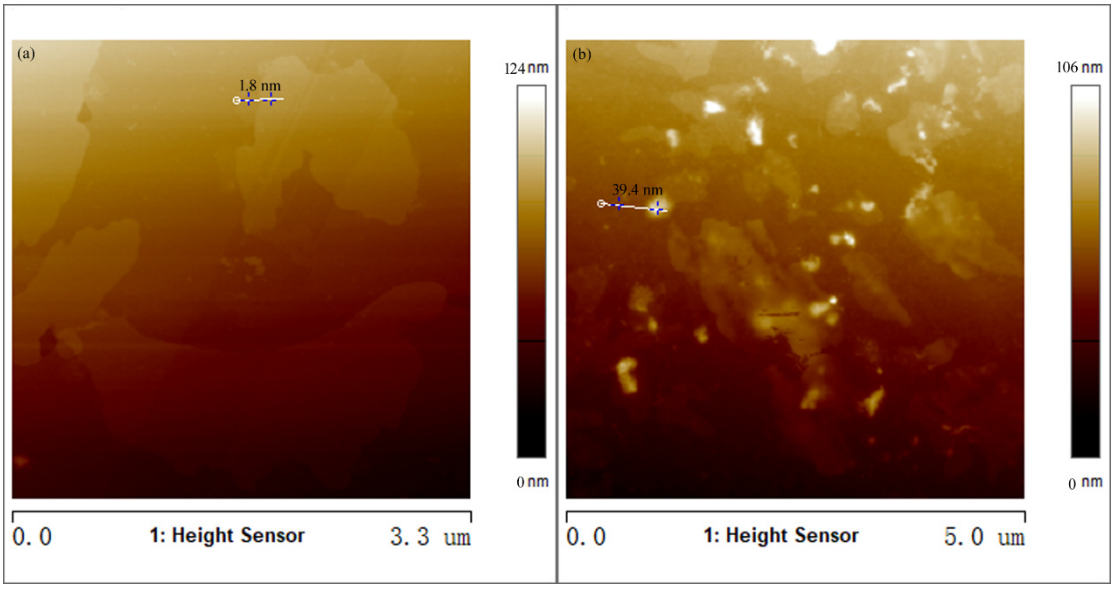

Fig. S1. AFM images of GO (a) and rGOA (b) sheets.

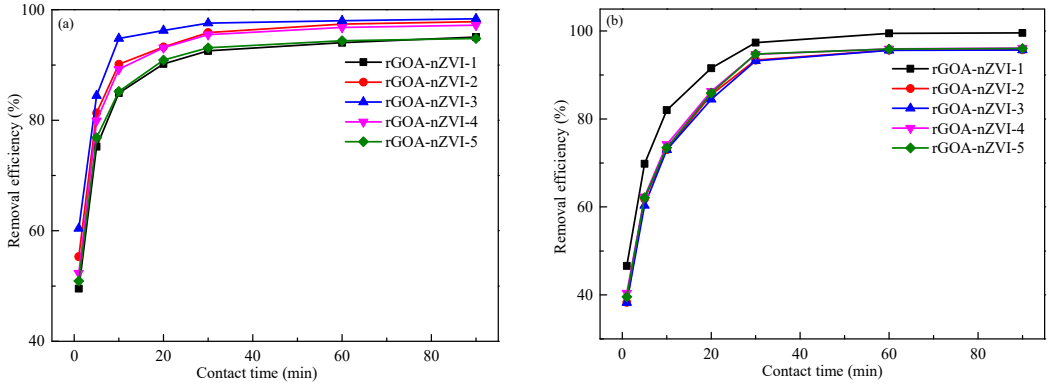

Fig. S2. MB removal (a) and MO removal (b) by rGOA-nZVI at different mass ratios of nZVI and rGOA.

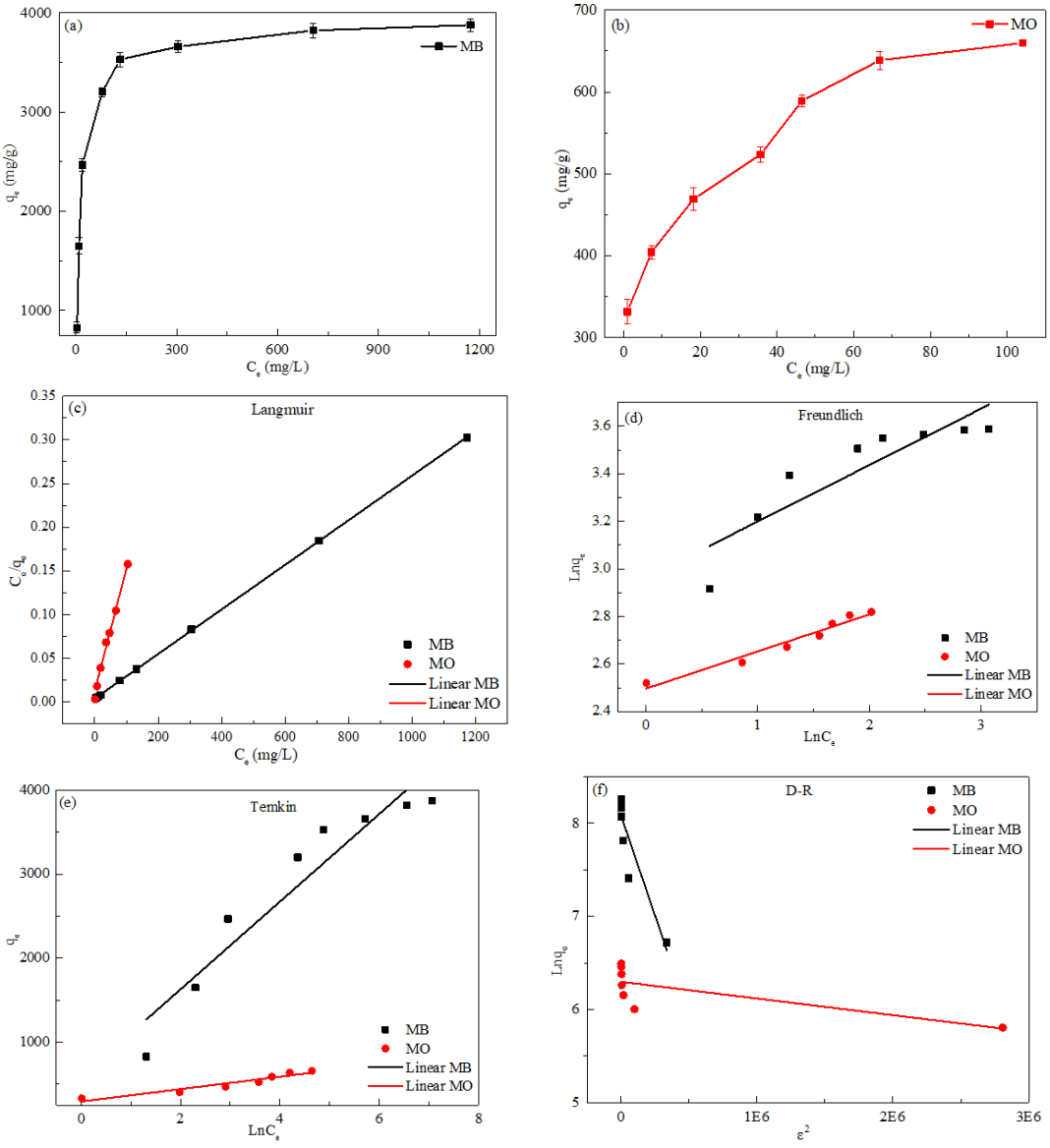

Fig. S3. The isotherm study (a and b) and isotherm models (c-f) of MB and MO removal by rGOA-nZVI composites. (Amount of rGOA-nZVI-1 and rGOA-nZVI-3 = 0.03 g, solution pH = 6.0, temperature = 25°C and contact time = 60 min).

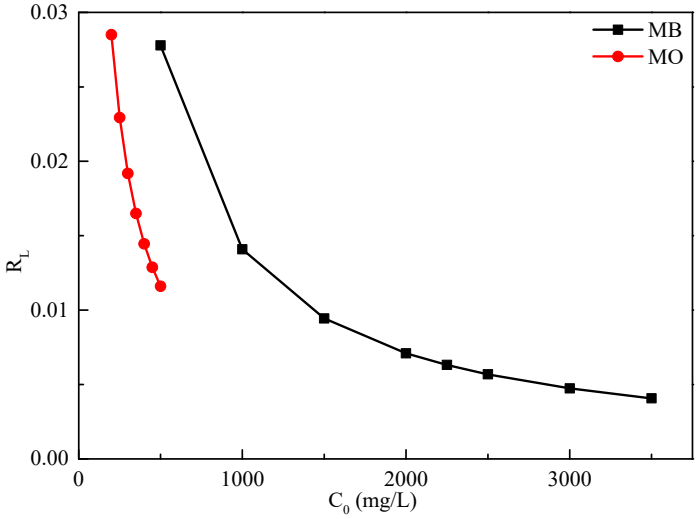

Fig. S4. Relationship between initial MB and MO concentrations and RL.

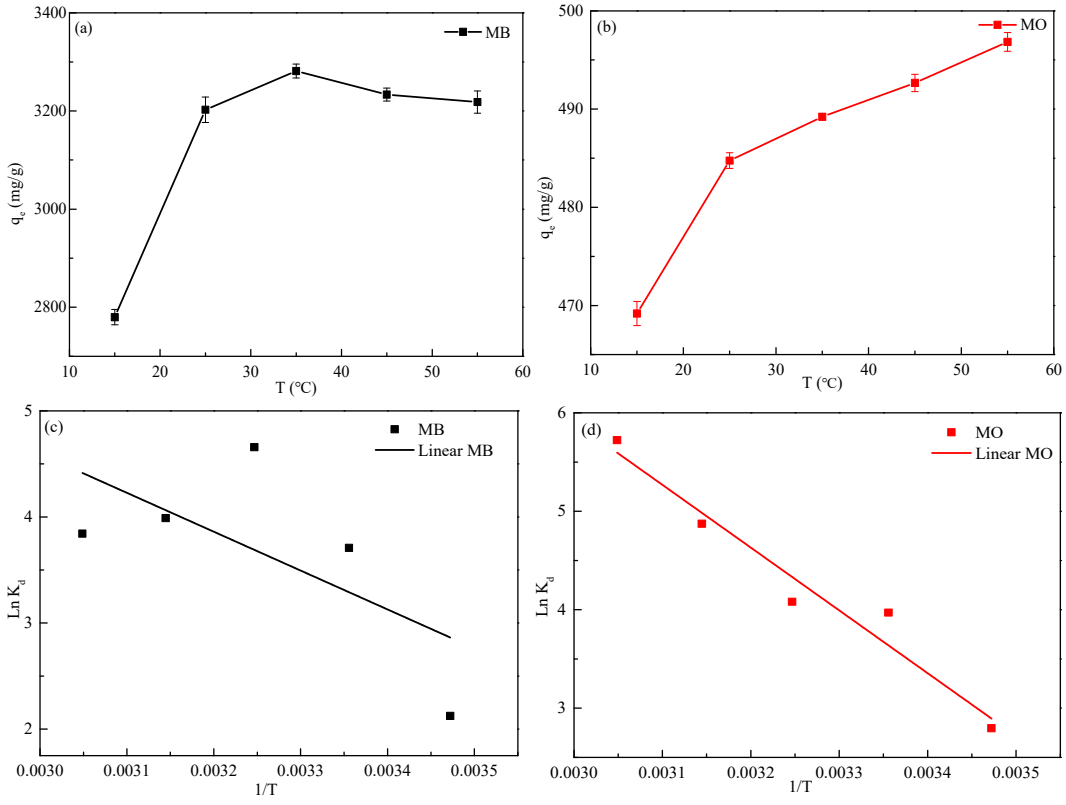

Fig. S5. (a) The effects of temperature on the MB removal by rGOA-nZVI-3 and(b) on the MO removal by rGOA-nZVI-1; (c) a linear plot of ln Kd against 1/T for MB; (d) a linear plot of ln Kd against 1/T for MO.

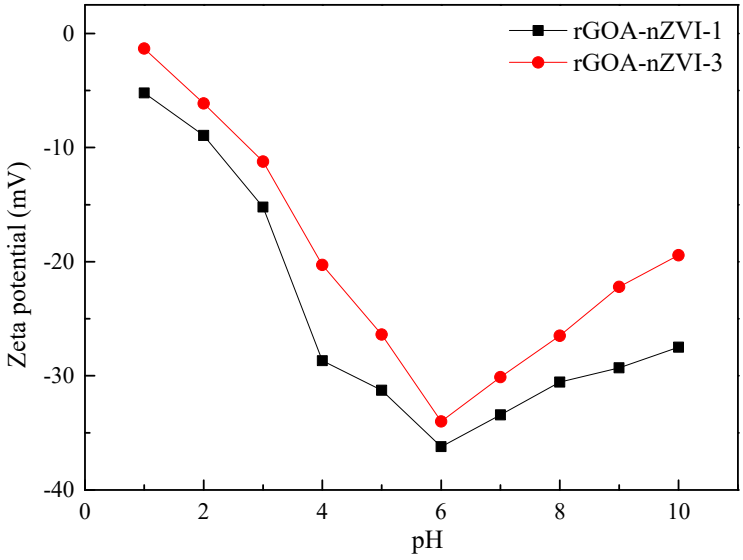

Fig. S6. Zeta potential of rGOA-nZVI-1 and rGOA-nZVI-3 dispersed in ethanol solutions from pH 1 to 10.

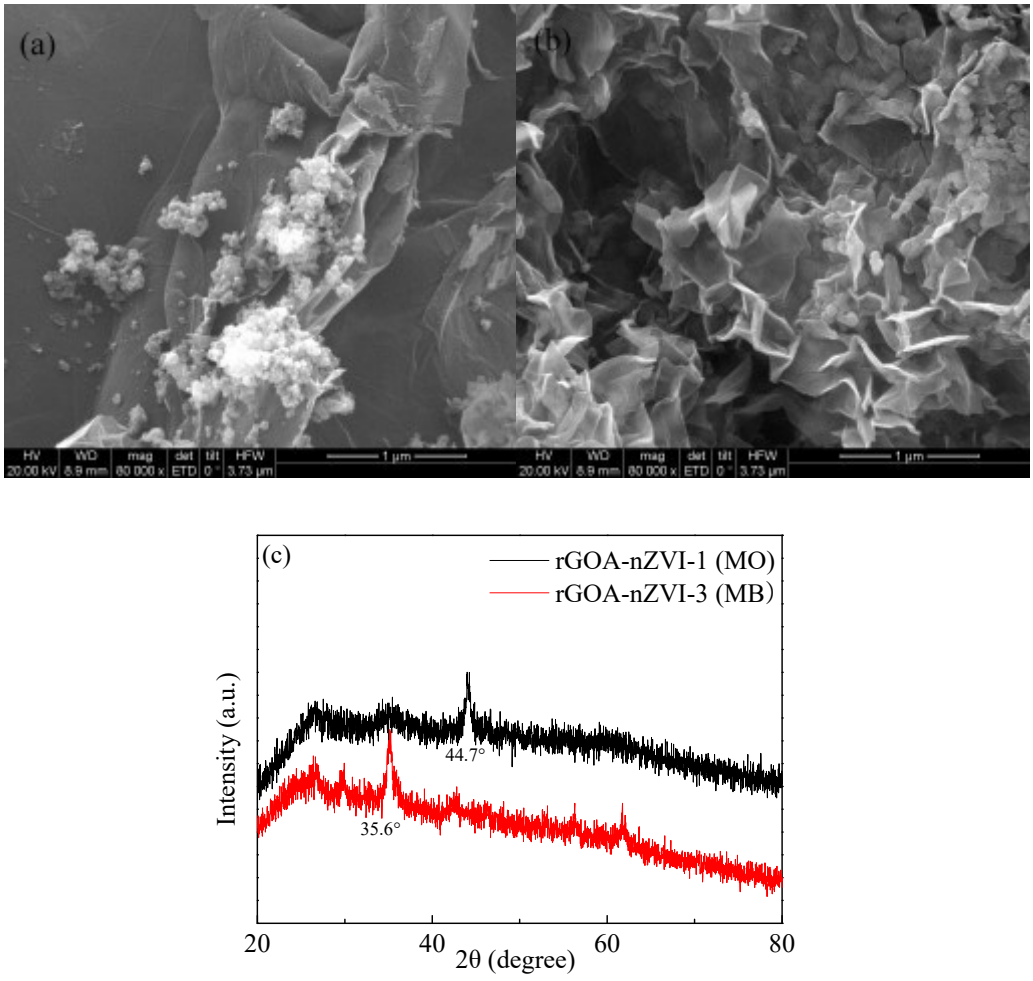

Fig. S7. The SEM images of (a) rGOA-nZVI-3 after removal of MB, (b) rGOA-nZVI-1 after removal of MO, (c) the XRD patterns of rGOA-nZVI-3 and rGOA-nZVI-1 after removal of MB and MO.

References

1. Liu JF, Chen JJ, Jiang L, Yin X. Adsorption of mixed polycyclic aromatic hydrocarbons in surfactant solutions by activated carbon. *J. Ind. Eng. Chem.* 2014;20:616-623. https://doi.org/10.1016/j.jiec.2013.05.024
2. Liu F, Chung S, Oh G, Seo TS. Three-dimensional graphene oxide nanostructure for fast and efficient water-soluble dye removal. *ACS Appl. Mater. Inter.* 2012;4:922-927. https://doi.org/10.1021/am201590z
3. Varadwaj G, Oyetade O, Rana S, Martincigh B, Jonnalagadda S, Nyamori V. Facile synthesis of three-dimensional Mg-Al layered double hydroxide/partially reduced graphene oxide nanocomposites for the effective removal of Pb^{2+} from aqueous solution. *ACS Appl. Mater. Inter.* 2017;9:17290-17305. https://doi.org/10.1021/acsami.6b16528
4. Shi YC, Wang AJ, Wu XL, Chen JR, Feng JJ. Green-assembly of three-dimensional porous graphene hydrogels for efficient removal of organic dyes. *J. Colloid Interf. Sci.* 2016;484:254-262. https://doi.org/10.1016/j.jcis.2016.09.008
5. Erenturk S, Malkoc E. Removal of lead(II) by adsorption onto Viscum albumL.: effect of temperature and equilibrium isotherm analyses. *Appl. Surf. Sci.* 2007;253:4727-4733. https://doi.org/10.1016/j.apsusc.2006.10.042